ACSNANO
www.acsnano.org
ARTICLE

Designer Dual Therapy Nanolayered Implant Coatings Eradicate Biofilms and Accelerate Bone Tissue Repair

Jouha Min,[†,‡] Ki Young Choi,[†,‡] Erik C. Dreaden,[†,‡] Robert F. Padera,[§,∥] Richard D. Braatz,[†] Myron Spector,[§,⊥,#] and Paula T. Hammond*[,†,‡]

[†]Department of Chemical Engineering, Massachusetts Institute of Technology, Cambridge, Massachusetts 02139, United States
[‡]Koch Institute for Integrative Cancer Research, Massachusetts Institute of Technology, Cambridge, Massachusetts 02139, United States
[§]The Harvard-MIT Division of Health Sciences and Technology, Massachusetts Institute of Technology, Cambridge, Massachusetts 02139, United States
[∥]Department of Pathology, Brigham and Women's Hospital, Boston, Massachusetts 02215, United States
[⊥]Department of Orthopedic Surgery, Brigham and Women's Hospital, Boston, Massachusetts 02115, United States
[#]Tissue Engineering Laboratories, VA Boston Healthcare System, Boston, Massachusetts 02130, United States

Supporting Information

ABSTRACT: **Infections associated with orthopedic implants cause increased morbidity and significant healthcare cost. A prolonged and expensive two-stage procedure requiring two surgical steps and a 6−8 week period of joint immobilization exists as today's gold standard for the revision arthroplasty of an infected prosthesis. Because infection is much more common in implant replacement surgeries, these issues greatly impact long-term patient care for a continually growing part of the population. Here, we demonstrate that a single-stage revision using prostheses coated with self-assembled, hydrolytically degradable multilayers that sequentially deliver the antibiotic (gentamicin) and the osteoinductive growth factor (BMP-2) in a time-staggered manner enables both eradication of established biofilms and complete and rapid bone tissue repair around the implant in rats with induced osteomyelitis. The nanolayered construct allows precise independent control of release kinetics and loading for each therapeutic agent in an infected implant environment. Antibiotics contained in top layers can be tuned to provide a rapid release at early times sufficient to eliminate infection, followed by sustained release for several weeks, and the underlying BMP-2 component enables a long-term sustained release of BMP-2, which induced more significant and mechanically competent bone formation than a short-term burst release. The successful growth factor-mediated osteointegration of the multilayered implants with the host tissue improved bone-implant interfacial strength 15-fold when compared with the uncoated one. These findings demonstrate the potential of this layered release strategy to introduce a durable next-generation implant solution, ultimately an important step forward to future large animal models toward the clinic.**

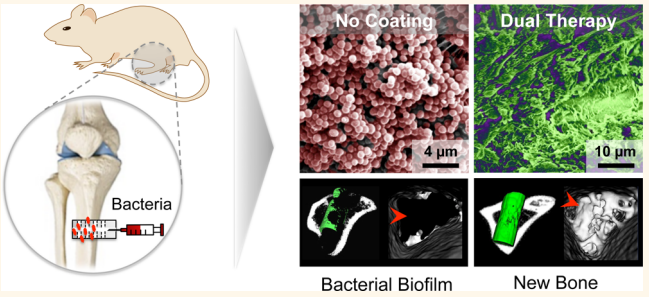

KEYWORDS: *antibacterial, regenerative medicine, nanolayered coating, layer-by-layer, controlled drug release, biomaterials, wound healing*

Infection associated with prosthetic joints, in particular osteomyelitis, is by far the most common reason for complications which often lead to their removal (74.3%),[1] sometimes requiring multiple revision surgeries and amputation in severe cases. Infection significantly increases time to heal and patient morbidity, and places huge financial burdens on the patient and the healthcare system—projected to exceed $1.62 billion/year by 2020.[2] Implant-related infections are typically caused by microorganisms growing in a hydrated matrix of their own synthesis, known as biofilms. Biofilms develop preferentially on inert surfaces and, thus, occur commonly on medical devices. Bacterial cells in biofilms can withstand host immune

Received: January 5, 2016
Accepted: February 28, 2016

DOI: 10.1021/acsnano.6b00087
ACS Nano XXXX, XXX, XXX−XXX

Scheme 1. Programmed Sequential Dual Therapy Delivery Strategy To Win the "Race to the Surface" against Bacteria[a]

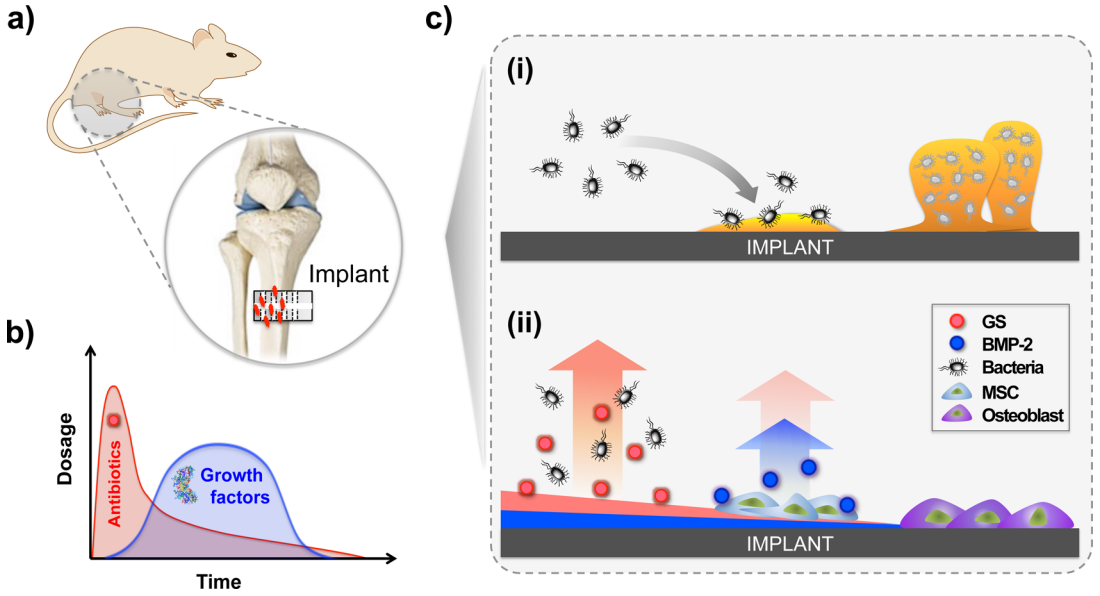

[a](a) Illustration of rat tibia model with induced osteomyelitis. (b) Desired release profile of an antibiotic and a growth factor and illustration of the top-down degradation of a LbL coating on an orthopedic implant. (c) Possible scenarios following *in vivo* application (i) In an uncoated implant, the residual bacteria in the defect and avascular tissue act as foreign bodies and can cause reinfection and form biofilm (represented by the yellow area). (ii) In our dual therapy LbL coating, however, local delivery of an antibiotic (red circles) controls infection until the implant is vascularized and immune-competent. The subsequent release of a growth factor (blue circles) induces the osteogenic differentiation potential of endogenous precursor bone marrow stem cells, resulting in optimal bone healing and bone-implant integrity.

responses, and they are much less susceptible to antibiotics than their nonattached individual planktonic counterparts.[3] For this reason, biofilm infections are difficult to truly eliminate and, typically, show recurring symptoms, even after cycles of antibiotic therapy.

Revision arthroplasty, in which an implant must be removed and replaced due to infection, loosening, or other medical complications, calls for the elimination of existing/potential infection, followed by the promotion of bone growth and vascularization of bone tissue, both of which are critical to the healing and regrowth of bone.[4] In the U.S., the prolonged and expensive two-stage procedure requiring two surgical steps and a 6− 8 week period of joint immobilization has been the only viable option for revision arthroplasty of an infected prosthesis for the past three decades.[5] An alternative approach to the suboptimal two-stage revision is a single-stage surgical exchange using a drug-device combination system. Currently, this approach has been attempted using antibiotic-impregnated polymeric bone cement,[6,7] but these systems are limited in the amount of antibiotic that can be loaded without compromising mechanical properties, thus limiting the ability to address existing infections. Drug loaded bone cements have a number of other disadvantages: harsh setting conditions required within the patient's tissue,[8] low control of release kinetics leading to primarily bolus release and its potential adverse effects at high-dose,[6,9] and retarded bone repair, less effective remodeling of bone and a slow and more painful patient recovery.[10] These issues, especially bone repair, become particularly acute for obese and diabetic patients on immunosuppressive therapy.[11,12] Also, in elderly patients the danger of brittle fracture due to osteoporosis and slower rate of wound healing compounds the complexity of such a procedure.

To address these issues, we sought to explore a new means of generating thin film coatings for sequential delivery of antibiotics and osteoinductive growth factors from surfaces using the enabling nanofabrication tool of electrostatic multilayer assembly to create conformal nanoscale coatings in a layer-by-layer (LbL) fashion;[13] LbL films can embed large weight fractions of biologic cargos.[14] This goal is accomplished by alternating charged drugs with degradable polyions such that complex, multicomponent release of drugs takes place from implant surfaces. Unlike more traditional polymeric delivery systems like poly(methyl methacrylate)-based bone cement, LbL assembly can be used to achieve high loadings of drug within a nanoscale conformal film that easily coats porous or nonporous substrates of all kinds.[15−17] The resulting nano- to micron scale coating can achieve independently tuned multi-drug release kinetics, while avoiding harsh fabrication conditions that significantly lower the activity of biologic drugs. Recently, studies have shown that the delivery of an anti-infective in conjunction with osteogenic growth factor can lead to more rapid healing of bone in animal bone fracture models.[18,19] Even following extended antibacterial treatment, there is the potential for residual bacteria to remain within the bone, and without the aid of an osteoinductive agent, bacteria "race to the surface"[20] to colonize the implant−bone interface, arriving at the free surface and rapidly generating a biofilm before mesenchymal precursors can arrive to attach and begin to generate bone. The use of an osteogenic growth factor can resolve this issue by inducing significant numbers of osteoblasts[21] and facilitating their rapid integration at the materials interface.[22] If the race is won by tissue, and stable integration is established, then the surface becomes less available for bacterial colonization.[23]

Although there are advantages to combining delivery of antibiotics and growth factor proteins, it is not straightforward to devise a singular materials system that is capable of high loading of these very different molecules while achieving

DOI: 10.1021/acsnano.6b00087
ACS Nano XXXX, XXX, XXX−XXX

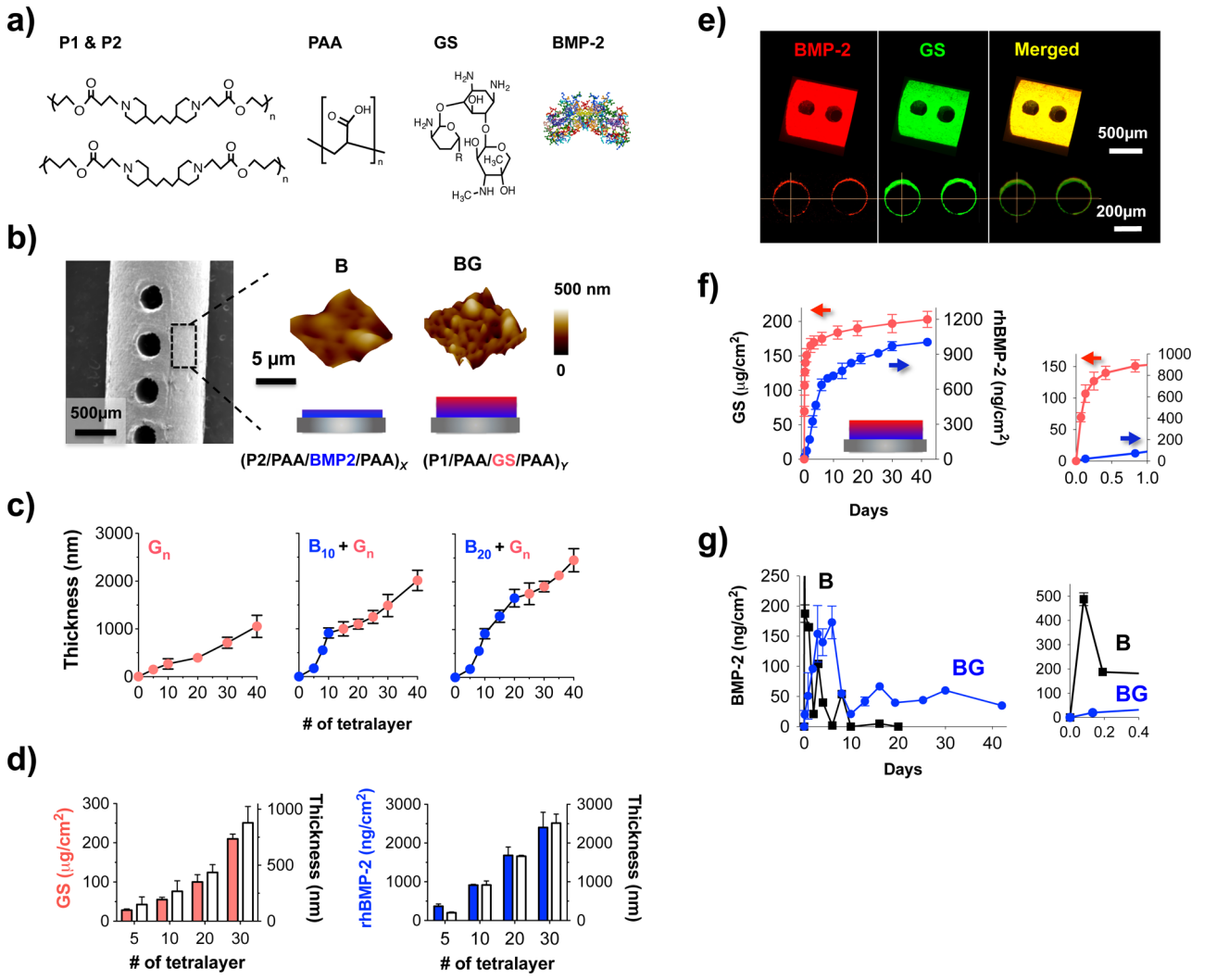

Figure 1. Designer dual therapy implant coatings for antibacterial treatment and bone regeneration. (a) Molecular structure of materials in the system. (b) SEM image of a PEEK implant with drilled channels, film composition formula for B and G components, and AFM height 3D images of B_{10} and $B_{10}G_{20}$ coated implants. (c) Growth curve of BG coatings as a function of tetralayer number. (d) Loadings and corresponding film thicknesses of BG coatings. (e) Representative confocal images of $B_{30}G_{30}$ coated implants with Alexa647-BMP-2 (red) and Alexa488-GS (green) (top, surface; bottom, cross sections of implant channels; scale bars, 250 μm). (f) Cumulative release profiles of GS (red circles) and BMP-2 (blue circles) from implants coated with $B_{10}G_{20}$. (g) The increment of BMP-2 release from implants coated with B_{10} (black circles) and $B_{10}G_{20}$ (blue circles) measured between each time point.

independently controlled and sustained release of both. Furthermore, incorporation of biologic drugs requires a solvent-free, low temperature method to avoid denaturation, which further limits the choice of materials as carriers. Ultimately, an implant coating that can be implemented directly onto the prosthesis surface would be most efficacious and convenient for implementation for surgical use, and would retain the mechanical properties of the implant and the nature of the bone−implant interface. We developed a defense strategy (Scheme 1a,b) to win the race against invading pathogens focused on incorporating (i) gentamicin sulfate (GS), the most commonly used aminoglycoside antibiotic with broad bactericidal spectrum, and (ii) bone morphogenetic protein (BMP-2), one of the most prominent osteoinductive growth factors used in clinic,[24,25] in a degradable multilayer coating, which provides localized release of the two therapeutics in the biologically relevant time scales needed for each to create a bacteria-free and bone-inducing microenvironment (Scheme 1b).[26] We established a rat tibia model with induced osteomyelitis to examine whether the LbL film can treat an established infection, while actively providing the biochemical cues to accelerate bone repair. In this study, we used luciferase encoding *Staphylococcus aureus* Xen 29 whose resistance against GS is 20-fold higher than general strains of *S. aureus*, the most common pathogen causing osteomyelitis, enabling a more rigorous evaluation of our approach (Figure S1). We demonstrated that the dual therapy approach allowed eradication of biofilms and control of the bone-regenerative process, and thus optimal integration with new healthy bone within a few weeks.

RESULTS AND DISCUSSION

Programmable Dual Therapy Implant Coating. We used LbL deposition to fabricate a dual therapy multilayer system consisting of an underlying BMP-2 releasing component and a top layer of GS releasing component on radiolucent cylindrical-shaped PEEK implants (1.3 mm in diameter, 4 mm in length, see Figure 1) with lateral channels of 250-μm in

DOI: 10.1021/acsnano.6b00087
ACS Nano XXXX, XXX, XXX−XXX

diameter, the optimal pore size for vascular invasion and ingrowth of mineralized bone.[27] For the BMP-2 component, P2 was alternated with poly(acrylic acid) (PAA) and BMP-2 in the form of $[Poly2/PAA/BMP\text{-}2/PAA]_X$ or B_X tetralayers (Figure 1a,b). Next, we deposited the overlying GS component with P1, PAA and GS alternated in the form of $[Poly1/PAA/GS/PAA]_Y$ or G_Y. Key to this film composition is that P1 ($t_{1/2}$ < 5 h) and P2 ($t_{1/2}$ ~ 40 h) undergo hydrolytic degradation at different rates under physiological conditions,[28] thus allowing the release kinetics to be tailored separately and enabling the staged first-order or pseudo-zero-order release of GS and BMP-2. Previous studies have demonstrated the biocompatibility of the polymers *in vitro* and *in vivo*.[29,30] Consistent with these data, we observed no apparent local toxicity or inflammation in any of the rats treated throughout these studies (Figure S2).

Profilometry measurements performed on LbL films constructed in parallel on Si substrates showed linear multilayer growth of GS component with increasing deposition cycles (Figure 1c). Measurement of GS recovered from coatings disrupted by treatment with sodium chloride showed ~7 μg of GS deposited per tetralayer per cm^2 of surface area (Figure 1d). Measurement of the BMP-2 component showed a delayed linear growth with an induction stage, after which the thickness and loading increase becomes linear (~80 ng/tetralayer/cm^2). For the dual therapy film, the GS linearly increased with increasing rounds of tetralayer deposition, confirming linear film growth atop the BMP-2. The fitted linear equation for GS loading has a nonzero *y*-intercept likely due to interpenetration of small molecular GS into the underlying BMP-2 layers, thus increasing loading. Confocal imaging of BG coated implants showed conformal colocalized fluorescence from BMP-2 and GS over the surface and inside channels of each implant (Figure 1e) with a slightly thicker layer of GS when compared to BMP-2, indicating interdiffusion of GS into the underlying B component. (Individual LbL components were too thin to resolve as distinct layers.) The surface morphology of the coatings on PEEK implants was examined using atomic force microscopy (AFM) and scanning electron microscope (SEM). AFM measurements gave RMS roughness values of 57 ± 17 and 120 ± 23 nm for the B and BG films, respectively. A noticeable difference in surface morphology was observed in the AFM topology (Figure 1b) and SEM images (Figure S3); the B-coated film shows a smooth and homogeneous morphology, whereas the BG-coated film with outermost GS layers displays a rougher morphology likely due to a high segmental density of loops and tails of high molecular weight PAA in the G component.

To test release kinetics, implants coated with BG films were immersed in pH 7.4 PBS at 37 °C for varying times (Figure 1f). For GS, we observed first-order release kinetics with minimal burst release at 60 μg/cm^2/day for the first day followed by a sustained release at 1.0 μg/cm^2/day, which remains above minimum inhibitory concentration (MIC) until complete elution; this profile is highly desired and advantageous because it can lower the chances of developing antibiotic resistance of bacteria and adverse effects on osteogenesis at elevated levels.[26] By contrast, BMP-2 release exhibited a relatively slow and continuous two-phase release over extended periods: diffusion-controlled release at 110 ng/cm^2/day for the first 6 days, followed by degradation-controlled release at ~13 ng/cm^2/day until complete elution at 40 days. The ionically cross-linked and densely packed GS layers played a role as a barrier, reducing the release rate of BMP-2 in early times as shown in Figure 1g; the relevant release time of the BG films ($t_{70\%}$ ~ 10 days) was 10-fold greater than that of single-drug B films ($t_{70\%}$ < 1 day). The sustained release of BMP-2 is more favorable than a short-term release at high doses because of rapid clearance from the target[31] and quantities far above physiological levels resulting in a suboptimal impact on tissue regeneration and serious side effects such as bone cancer.[32] In general, slower release of therapeutic molecules are anticipated *in vivo* compared to *in vitro* due to a slow clearance rate, an overall accumulation, lower hydrolysis rate owing to the adsorption of proteins, and shifts in pH in the infected environment at the implant site.[33,34]

For further assessment, the *in vivo* local concentrations were estimated using the *in vitro* release data. Assuming that the effective control volume is the bone marrow space (V ~ 0.1 mL, set as an upper bound), we roughly estimated the temporal concentrations at varying clearance and cell uptake rates, and predicted the local concentrations to be within therapeutic windows (0.15−300 μg/mL GS and >100 ng/mL BMP-2)[35] in adapted time scales (Figure S4). The loading and release kinetics of the two drugs could be tuned by simply varying the number of deposited layers or by tuning the physical properties of the structural components (Figure S5). Each component can be reproducibly synthesized by physiochemical means—that is, the temporal separation between release of the two drugs can also be enhanced by using barrier layers between the two components, as previously reported.[36] This system can be easily extended to incorporate and deliver several antibiotics and growth factors together or in sequence. Together, these data show that the multilayer structure allows the individual kinetics of each drug's release to be easily tailored over days to weeks, indicating a wide applicability of this approach to diverse drug delivery applications.

Prior to *in vivo* evaluation, we tested and confirmed *in vitro* antibacterial activity of the dual therapy coating against *S. aureus* Xen 29, and osteogenic efficacy to induce differentiation of preosteoblast MC3T3-E1 cells (Figure S6). We also validated that, when delivered together in cocultures of *S. aureus* and MC3T3-E1—a better representation of the *in vivo* scenario—GS and BMP-2 maintain their primary therapeutic functions (Figure S6d). There was no apparent adverse effect associated with the composite film at these concentrations.

Rat Tibia Model with Induced Osteomyelits. Next, we developed an animal model with induced implant-centered infection to test the *in vivo* bioactivity of multilayer films with different formulations and evaluate its potential as a promising adjuvant therapy for revision arthroplasty after infections. In brief, we inserted a bare implant below the patella ligament in tibiae of adult male Sprague−Dawley rats, and inoculated by injecting 5 × 10^5 cfu of Xen 29 (Figure S7). We monitored the development of osteomyelitis using bioluminescent and radiographic imaging, and observed clinical signs of osteomyelitis—swelling and redness, biofilm, and bone destruction—(Figure S7b−d). At 7 days post-inoculation, we performed one-stage revision: removed the infected implant, debrided and irrigated the infected site, and then inserted a new implant. *In vivo* experiments involved 3 treatment groups with a control group of the untreated: uncoated, coated with B_{10}, G_{20}, or B_{10} + G_{20} (referred to henceforth as U, B, G, and BG, respectively).

***In Vivo* Antibacterial Treatment.** We first examined short-term antibacterial efficacy of multilayer coatings with different formulations. The control group U showed prolonged bioluminescence, peaking on day 4, then slowly decreasing to background levels by 14 days post-revision, demonstrating

DOI: 10.1021/acsnano.6b00087
ACS Nano XXXX, XXX, XXX−XXX

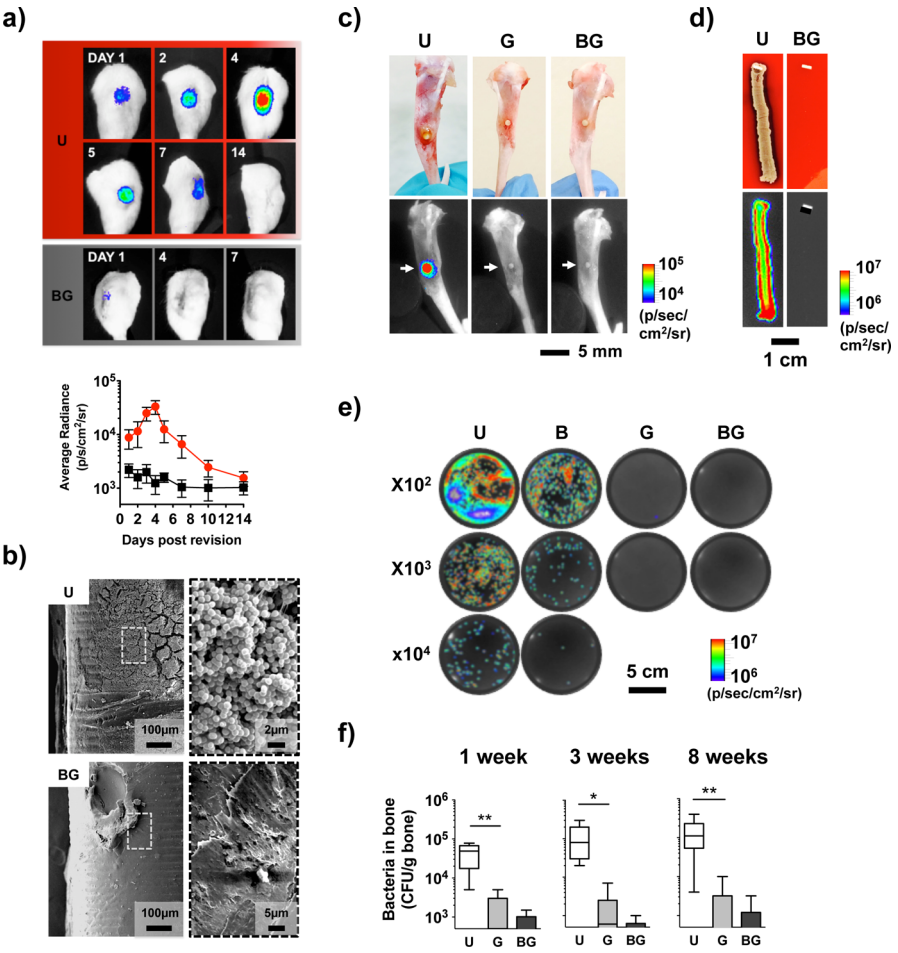

Figure 2. ***In vivo*** **and** ***ex vivo*** **antibacterial treatment. (a) Post-revision bacterial growth of bioluminescent** ***S. aureus*** **tracked by monitoring average radiance over time. Data represent the mean ± SEM,** $n = 3$**. (b) SEM images show presence of biofilm (consisting of spherical bacterial cells) on the uncoated, but prevention of reinfection on the coated after 3 weeks. (c) Representative images of tibiae treated with different films and harvested at 8 weeks after revision. (d) Rollover cultures of implants pulled out on day of sacrifice (8 weeks). The implant with GS has significantly less bacterial growth than the uncoated (**$P < 0.001$**). (e) Representative bioluminescence images of** ***S. aureus*** **recovered from tibiae harvested at 8 weeks, serially diluted, and cultured for viable plate count. (f) Box-and-whisker plot comparing colony-forming unit (cfu) recovery per gram of bone tissue at 1, 3, and 8 weeks post-revision. *$P < 0.05$, **$P < 0.01$, ***$P < 0.001$, ANOVA with Tukey** ***post hoc*** **test.**

proliferation and delayed resolution of residual bacteria at the implant site (Figure 2a). By contrast, the antibiotic treated (BG) had no detectable luciferase expression, indicating local antibiotic transport into the infected site. Note that the bioluminescent signal is not indicative of bacterial number, but a measure of bacterial metabolic activity resulting from the reaction of enzymes and protein substrates synthesized by the *lux* operon.[37] That is, the observed decrease after day 4 does not represent a reduction in bacterial number, but rather initiation of colonized bacterial growth (biofilm), which has a substantially lower metabolic rate. The SEM images of implants pulled out after 3 weeks showed clear evidence of biofilm on the uncoated (Figure 2b).

Next, we compared *ex vivo* bacterial responses in tibiae excised at 8 weeks post-revision to validate long-term antibacterial efficacy using bioluminescence imaging and *S. aureus* isolated from the surface of implants. The untreated tibiae showed strong bioluminescent expression, whereas the antibiotic treated tibiae led to no or very weak expression of *S. aureus* comparable to background at 8 weeks after revision, demonstrating elimination of the existing infection and strong defense against reinfection (Figure 2c). Roll-over cultures also showed the efficacy of the BG coating in preventing surface bacterial growth compared to the uncoated ($\gg 10^3$ cfu, implants were rolled on the blood agar in Figure 2d). To evaluate bacterial growth in the surrounding tissue, we used the viable plate counting method to quantify colony-forming unit (cfu) recovery per gram of bone harvested after 1, 3, and 8 weeks (Figure 2e). The quantity of bacteria recovered from the untreated tibiae was found to be 2−3 orders of magnitude greater than that recovered from the BG treated after 3 weeks ($P < 0.05$, Figure 2f). Further, MIC values of GS against bacteria isolated from treated tibiae were measured to be identical to the parental strain, confirming no development of antibiotic resistance (Figure S8). The maintenance of long-term antibacterial activity through host−implant integration is a promising result, particularly in the absence of detectable subclonal selection for resistance. Thus, our microbiological data show the potential of the dual therapy approach to match the potency of long-term antibiotic therapy during bone tissue regeneration.

Host−Implant Interaction at the Cellular Level. Parallel to bacterial treatment, another very important clinical challenge is tissue integration. We analyzed histological sections of

DOI: 10.1021/acsnano.6b00087
ACS Nano XXXX, XXX, XXX−XXX

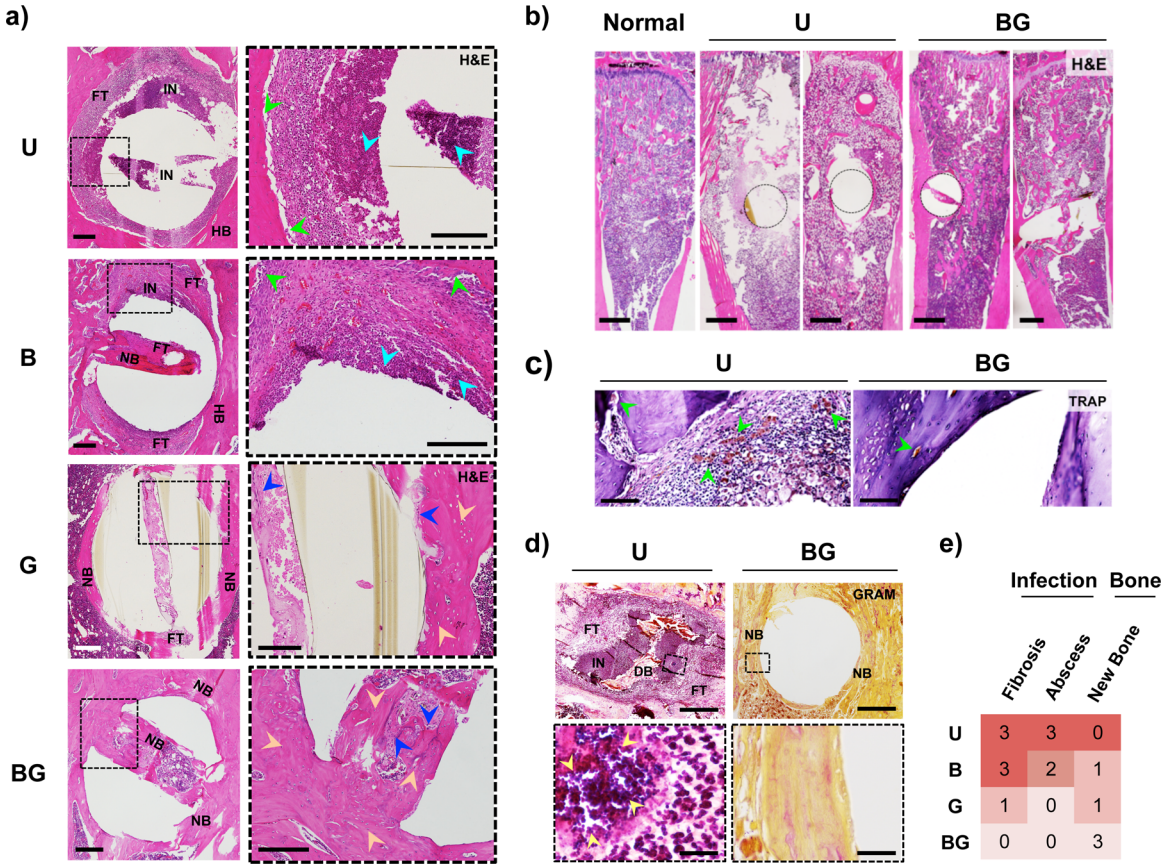

Figure 3. Histological effects of various implant coating formulations. (a) Representative hematoxylin and eosin (H&E) sections of tibiae with implants uncoated (U) or coated with B, G, or BG at 8 weeks post-revision at low (left) and high (right) magnification. Implants with gentamicin show significantly less chronic inflammation and more new bone. BMP-2 from the BG coated promoted visibly notable healing and complete bone ingrowth throughout the implant channels. (b) H&E sections of proximal metaphysis. (c) TRAP stained sections and (d) Gram stained sections of Group U and BG at 8 weeks post-revision. Scale bars, 200 μm (a), 1 mm (b), 500 μm, (c, top), and 20 μm (c, bottom). NB, new bone; HB, host bone; DB, dead bone; FT, fibrous tissue; IN, inflammation. Arrows: lime, osteoclasts; cyan, neutrophils; blue, osteocytes; orange, osteoblasts; yellow, *S. aureus*. (e) For the semiquantitative assessment of the severity of infection and lack of tissue integration, histological scores were determined based on the histological sections a–c (0, none; 1, few; 2, moderate/focal; 3, numerous and diffuse).

excised tibiae with intact implants to explore the underlying cellular processes at the implant site (Figure 3 and Figure S9). In the BG, complete bone deposition and host–implant integration with no signs of reinfection was observed at 8 weeks post-revision (Figure 3a). The new bone was laid down on the implants without any scar tissue or avascular capsule, continued to grow over time, and filled throughout the implant channels (Figure S10). Osteocytes and lamellar features of the newly synthesized bone around implants indicate bone maturation and restoration of most of the bone's original strength (Figure S11). By comparison, in the G, there were no indications of reinfection and fair, slower bone deposition on the implant surface, but retarded bone growth into the implant channels. In contrast, implants unequipped to fight against bacteria, U and B, showed bone destruction and adverse foreign body reactions as evidenced by dead bone or sulfur granules surrounded by a rim of neutrophils, lymphocytes, and foreign body giant cells, representing chronic osteomyelitis (Figure 3d and Figure S12). The B sample did exhibit some granulation tissue that penetrated the implant channels and supplied progenitor cells that progressively filled in the channels from the periphery and formed some bone tissue (Figure 3a). The observed complications in the U and B are related to the ability of *S. aureus* to trigger surrounding soft-tissue inflammation, incite bone destruction, and ultimately circulate *via* the bloodstream.[38] The histological analyses demonstrated that dual-delivery of an antibiotic and a growth factor is vital in both bacterial inhibition and bone tissue integration through maintenance of biologically adequate microenvironment for multiple weeks after revision.

Quantifying Bone Regeneration. To test the osteogenic ability of the dual therapy multilayer coating, we imaged and quantified temporal bone volume (BV) around the outer surface of implant and inside the channels using micro-computed tomography (μCT). Bone deposition was quantified at the regions of interest (ROIs, represented by the green cylindrical volume in Figure 4a) at 1, 3, 5, and 8 weeks post-revision. We observed that bony tissue regeneration was initiated at the cortical interface with the endosteal tissue and then extended to the surface in the medullary canal (Figure 4a and Figure S13). The volume and coverage of new bone around implants coated with G or BG generally increased over time, but much faster bone formation and remodeling was observed on the BG coated than others ($P < 0.01$); bone coverage of the BG coatings reached over 80% in 3 weeks (Figure 4b). The rate of bone penetration into the implant

DOI: 10.1021/acsnano.6b00087
ACS Nano XXXX, XXX, XXX–XXX

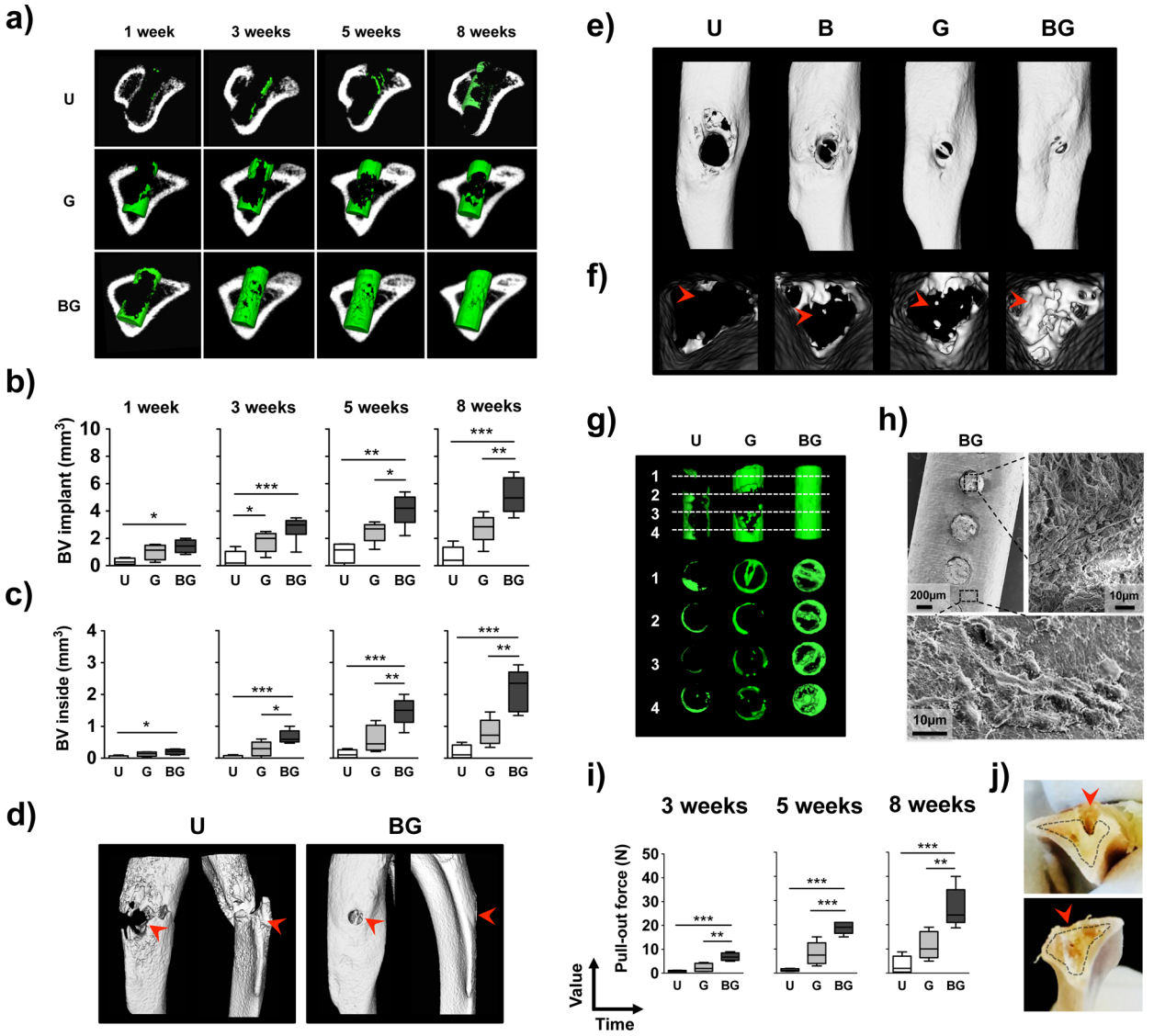

Figure 4. μCT imaging and quantification of bone healing and bone-implant integration. (a) Radiographs and 3D reconstruction of new bone around implants at 1, 3, 5, and 8 weeks after revision. (b–c) Quantitative healing indices derived from μCT measurements: bone volume around implants and inside the channels (using cylindrical ROIs in A). BMP-2 was critical for good healing. n = 4 per group. (d) In severe case of the untreated, substantial bone destruction led to bone fracture. (e) 3D images of front views, (f) top-down views in marrow space, and (g) implants show complete bone deposition on the BG. (h) SEM images of the BG coated implants pulled out at 8 weeks post-revision demonstrate tissue infiltration. (i) Box-and-whisker plot shows mechanical pullout force at predetermined time points, n = 4. (j) Bright-field images of excised tibiae treated with BG at 5 weeks post-revision. Red arrows denote implant sites. *P < 0.05, **P < 0.01, ***P < 0.001, ANOVA with Tukey *post hoc* test.

channels was at least 3-fold faster in the BG group, indicating early and rapid host–implant interlocking (Figure 4c and Figure S14). In contrast, substantial bone destruction was observed in the untreated (U and B), and in severe cases, it resulted in periprosthetic fracture or septic failure (Figure 4d). Osteomyelitis-dependent bone destruction can confound therapy by destroying the vascular architecture of infected bone and limiting antimicrobial penetration to the biofilm.[39] Additional μCT images of tibiae and implants in Figure 4e–i show (i) normal bone healing with no signs of infection in the antibiotic treated tibiae (G and BG), and (ii) complete bone coverage and penetration into the channels of the BG coated, confirming that controlled BMP-2 release is highly effective at enhancing osseointegration, especially in this challenging clinical scenario where the host bone is not optimal, that is, has a previous local infection with some infection-induced trauma to bone and soft tissue.

Comparison of Bone Mechanical Properties. We performed mechanical pull-out tests to quantify the interfacial strength of implants anchored/interlocked with the reconstructed bone. Parallel to bone tissue growth, the interfacial strength generally increased over time in all different groups, but the BG coated showed 10- to 15-fold higher shear strength than the uncoated implant (P < 0.001) and 3-fold higher than the single-drug GS coated (P < 0.01) up to 8 weeks after revision (Figure 4i and Table S1), confirming an important osteogenic role of BMP-2 in mediating early bonding between implants and host tissue. The interfacial strength of BG coated implants, calculated by dividing the pull-out force by the implant surface area, was found to be up to 17-fold higher than bioactive bone cements (0.07–0.9 MPa) and comparable to

DOI: 10.1021/acsnano.6b00087
ACS Nano XXXX, XXX, XXX–XXX

osteoconductive hydroxyapatite interfaces (0.5−1.5 MPa) in animals. SEM images of explants presented bone tissue on the surface and within the implant channels, indicating that the pull-out tests resulted in partial cohesive fracture of bone rather than complete adhesive failure at the implant-tissue interface (Figure 4h). The bone growth and mechanical data together demonstrate that the bony tissue formed with dual therapy BG layers was mature, organized, and cohesive enough to establish mechanical integrity of the reconstructed bone and implant, whereas no or very limited bone was regenerated with the uncoated or single-drug coated, resulting in a lower stiffness and thus premature failure.

CONCLUSIONS

One of the important problems in the field of orthopedic medicine is the ability to create a stable bone−materials interface with an implant, particularly when faced with the difficult condition of bone infection. Only recently have we come to understand the significance of addressing infection during the bone wound healing process; however, to apply this understanding toward an effective treatment requires the ability to locally deliver exacting amounts of therapeutics of different types over the appropriate timeframes. In this study, we created conformal, programmable, and degradable dual therapy multilayer coatings (0.5−2 μm thick) in a layer-by-layer (LbL) fashion using the enabling nanofabrication tool of electrostatic multilayer assembly. The nanolayered construct allows large loadings of each drug in a very thin film coating to provide sufficient treatment as well as independent control of release kinetics for each therapeutic agent in an infected implant environment. The architecture of the coatings was adapted to allow early release of antibiotics contained in top layers of the coating that eliminate a well-established bacterial biofilm, followed by sustained release above the MIC over several weeks; whereas, the underlying BMP-2 layers enabled a long-term sustained release of BMP-2, which induced much more significant, well-integrated, and more mechanically competent bone formation than a short-term burst release.

To illustrate the clinical translational potential of this approach for an optimal single-stage revision, we developed a rodent model with induced osteomyelitis, and used μCT analyses to quantify bone remodeling, namely pathologic bone destruction or growth factor mediated bone formation. The animal model demonstrates quantifiable differences in intraosseous bacterial survival and bone remodeling for multiple weeks, making it a valuable tool for study of later-stage assessment and for the development of new therapies. Furthermore, the surgical techniques are easily adaptable to other bacterial species, enabling study of new therapies using a variety of bone pathogens. The *in vivo* data demonstrated successful growth factor-mediated osteointegration of the multilayered implants with the host tissue (over 80% bone coverage within 3 weeks post-revision) and direct bone deposition after complete film degradation. The result was strong, long-term bone-implant integration, improving interfacial strength 15-fold when compared with the uncoated implant. The preclinical results in this study are deemed to outperform two-stage revision, a method currently viewed as a gold standard for revision after infection. Furthermore, the overlying antimicrobial coating is advantageous as a protection layer for feasible scale-up and shelf life extension as maintenance of absolute sterile conditions is nearly impossible.

We focused on dual delivery of an antibiotic and a growth factor owing to the urgent need for enhanced infection-reducing *and* tissue-integrating strategies in orthopedic application. However, the excellent flexibility of multilayers for incorporation and controlled release of diverse therapeutics suggests this approach should be also applicable to different medical devices such as vascular graft and artificial heart implants for which the risks of infection have not been fully addressed. Although further preclinical testing would be needed in a larger animal model, the data shown here collectively suggest that the programmable dual therapy multilayer coating is a promising approach to enable single-stage revision with minimal risk of reinfection and loosening, and thus the extended use of implants. This simple, safe, and economical technology has the potential to be applied in broad biomaterial and implant applications, to directly benefit the rapidly growing current and future generations of patients relying on prosthetic joints and other implants.

MATERIALS AND METHODS

Materials. Poly(β-amino esters), Poly1 (15 kDa), and Poly2 (20 kDa), were synthesized as previously reported.[40] BMP-2 was provided by Pfizer. PEEK (McMaster-Carr) was machined into implants with 1.3 mm of diameter, 4 mm of length, and 0.25 mm drilled channels. Materials were purchased from Sigma unless otherwise noted.

Polymer Multilayer Coating Preparation. LbL multilayer films were assembled using a Carl Ziess HMS-DS50 stainer. Films were constructed on Si wafers and PEEK implants following oxygen plasma treatment for 1.5 and 10 min, respectively. [Poly2/PAA/BMP-2/PAA] layers (B) were deposited through alternative immersion into Poly2 (1 mg mL^{-1}, pH 5.0), PAA (M_w ~ 450 kDa, 1 mg mL^{-1}, pH 5.0), and BMP-2 (40 μg/mL, pH 4.0) for 5 min, separated by two 1 min water rinses. [Poly1/PAA/GS/PAA] multilayers (G) were deposited similarly, alternating 5 min dips in Poly1 (1 mg mL^{-1}, pH 5.0), PAA (M_w ~ 1.25 MDa, 1 mg mL^{-1}, pH 5.0), and GS (10 mg mL^{-1}, pH 5.0), separated by two 1 min water rinses. Films were characterized using a Veeco Dektak profilometer. The surface morphology and roughness of the multilayer coatings on PEEK implants were observed using an atomic force microscope (Nanoscope IIIa; Digital Instruments) in tapping mode and a scanning electron microscope (JEOL JSM-6700F). Release kinetics and *in vitro* bioactivity characterization are described in the Supporting Information.

Animal Studies. All animal procedures were approved by the Institutional Animal Care and Use Committee at Massachusetts Institute of Technology (MIT). Adult male Sprague−Dawley rats (350−400 g; Charles River) were anesthetized and both lower limbs were shaved, disinfected with povidone iodine, and draped in a sterile manner. A 5 mm skin incision was made at the tibial metaphysis or diaphysis in the region of the tibial tuberosity and extended to the underlying fascia and periosteum. The implant site was prepared by intermittent drilling a 1.4 mm unicortical hole through the cortical and cancellous bone below the patella ligament in order to gain access to the medullary cavity. The drilling used a customized hand-held drill (Aseptico) with dental burrs (FST), operated at a low rotary speed with saline irrigation. The implant (diameter of 1.3 mm, length of 4 mm) with drilled holes (diameter of 0.25 mm) was inserted without tapping and was flush with the external surface of the tibia entry site. Bacteria inocula (5×10^5 cfu in 5 μL PBS) were delivered through the implant hole using a 25-μL microsyringe (Hamilton) into the medullary cavity. Controls received identical amounts of sterile PBS into identical types of implants. The outer opening of the implant cavity was sealed with bone wax. The incision was closed in two layers with 5−0 polyglycolic acid sutures (Vicryl) in subcutaneous tissues and skin, respectively. This procedure was repeated in the opposite limb. Animals were allowed unrestricted activity upon recovery and provided with analgesics. Detailed surgical procedure is provided in the Supporting Information.

DOI: 10.1021/acsnano.6b00087
ACS Nano XXXX, XXX, XXX−XXX

Rationale and Study Design. There were a total of four experimental groups with at least 12 test samples per group: uncoated (U), coated with B_X (B), G_Y (G) or B_X + G_Y (BG). To determine the study group size, we conducted power analysis with G*Power Analysis, using repeated-measures ANOVA, between-factors test. We assumed an effect size (f) of 0.5, an α error probability of 0.05, a power of 0.95, and a correlation of 0.2. Each animal has one implant in each leg (considered independent). Within each group, at least four implants were used for each measurement (IVIS, microorganism analysis, pull-out shear testing, and microCT) per time point. Some samples were used for representative histology. End points were predetermined to study the temporal effect of coatings of bone formation and implant integration. All experiments were randomized and nonblinded.

***S. aureus* Strain and Bacterial Inoculum.** All experiments were conducted with bioluminescent strain of *S. aureus* Xen 29 (derived from ATCC 12600; Xenogen). Bacterial strains were routinely grown on Luria-broth (LB) solidified with 1.5% agar at 37 °C or LB with shaking at 200 rpm, unless otherwise indicated. Bacterial inocula were prepared by 1:50 subculture of overnight LB cultures followed by growth at 37 °C and 200 rpm shaking for 3−6 h. Bacteria were collected by centrifugation, washed with PBS twice, and resuspended to a concentration of 1×10^8 cfu/mL in PBS.

Microbiological Evaluation. The implants were explanted, rolled over on trypticase soy agar plates with 5% sheep blood (VWR), and incubated overnight to determine the qualitative extent of surface colonization. The explanted bones were weighed, snap-frozen in liquid nitrogen, and homogenized using a BioPulverizer (BioSpec). The well-mixed powder was then added to 20 mL of sterile PBS, vortexed vigorously for 30−60 s, serially diluted, and plated to determine the concentration of bacteria in the homogenate (cfu/g). Plates with the largest countable number of bacteria were used in the statistical analyses. Antibiotic resistance was checked by growing overnight cultures of bacteria from homogenates and determining MICs according to a previously published microdilution procedure.[36]

microCT Analysis. Anesthetized live animals were imaged with a microCT (eXplore CT120, GE Medical Systems). Scanning protocol, shutter speed (325 s); 2 × 2 binning; 120 kV, 40 mA; 720 images; 0.877° increments; gain, 100; and offset, 20. Images were reconstructed and analyzed with MicroView (GE Healthcare). A threshold value and ROI were chosen by visual inspection of images (constant for all groups), and bone volume (BV) was measured.

Pull-Out Tensile Testing. After euthanasia, tibiae were explanted and stored in phosphate-buffered saline for immediate mechanical tensile testing (Instron 5943). The exposed head of the implant was connected to a load cell and was then subjected to a constant pull rate of 0.1 N/s. The pull-out force, parallel to the long axis of implant, was the maximum load achieved before implant detachment because of failure. Interfacial shear strength was calculated by dividing the pull-out force by the total surface area of the implant (25 mm^2).

Histology. After euthanasia, tibiae were explanted and were fixed in 4% paraformaldehyde (PFA). PFA-fixed tibiae with implants were partially decalcified for about 6 h with a rapid decalcifying formic acid/hydrochloric acid mixture (Decalcifying Solution, VWR) or for about 2 weeks with neutral EDTA solution, and embedded in paraffin wax. Sections (5 μm) of the bone−implant interface were stained with hematoxylin and eosin (H&E), Masson's trichrome, tartrate-resistant acid phosphatase (TRAP), and gram stains. Implants were embedded in glycol methacrylate (JB-4 Plus, Polysciences) following the manufacturer's protocol and sectioned. Cell lineages were identified with the help of Dr. Spector, Dr. Bronson, and Dr. Padera.

Statistical Analysis. All data analysis was performed in Prism 5 (GraphPad). Data are reported as mean ± standard deviation of a minimum of 3 samples. Statistical significance ($P < 0.05$) was determined using one-way ANOVA with a Tukey *post hoc* test.

ASSOCIATED CONTENT

Supporting Information

The Supporting Information is available free of charge on the ACS Publications website at DOI: 10.1021/acsnano.6b00087.

Methods, MIC of gentamicin against Xen 29, histology data for biocompatibility, SEM images of LbL-coated implants, rough estimate of drug concentration *in vivo*, *in vitro* release kinetics data, *in vitro* bioactivity evaluation, rodent model of implant-related infection, bacterial resistance test, histology (bright field and birefringence), microCT imaging and quantification of new bone formation, interfacial shear strength (PDF)

AUTHOR INFORMATION

Corresponding Author

*E-mail: hammond@mit.edu.

Author Contributions

J.M., M.S., and P.T.H. designed the experiments. J.M, K.Y.C., and E.C.D. carried out *in vitro* film characterization. J.M. carried out *in vivo* prosthesis-related infection studies using rodent tibial model. J.M., R.F.P., M.S., and P.T.H. analyzed the radiographic and histological data. J.M., R.D.B., and P.T.H. wrote the paper.

Notes

The authors declare no competing financial interest.

ACKNOWLEDGMENTS

This work was partly supported by the National Institutes of Health, National Institute of Aging (5R01AG029601-03). We thank N. Shah, Ph.D. for consultation on *in vivo* experiment design, R. Bronson, Ph.D. for analysis of histological sections, and M. Bauer for special histology staining. We thank the MIT Koch Institute Swanson Biotechnology Center, which is supported by the Koch Institute Core Grant P30-CA14051 from the NCI, for the use of facilities, and specifically the Hope Babette Tang (1983) Histology Facility and The Animal Imaging & Preclinical Testing Core Facility. The authors wish to express their appreciation to the Institute for Soldier Nanotechnologies at MIT, supported by the Army Research Office and Army Research Laboratories, whose facilities and equipment were used to conduct the research reported in this paper. We thank the Robert Langer Laboratory for the use of liquid scintillation counter and Instron, as well as the Tyler Jacks Laboratory for the use of Nikon light microscope. We also acknowledge Pfizer. Inc. for rhBMP-2.

REFERENCES

(1) Bozic, K. J.; Kurtz, S. M.; Lau, E.; Ong, K.; Vail, T. P.; Berry, D. J. The Epidemiology of Revision Total Hip Arthroplasty in the United States. *J. Bone Surg.* **2009**, *91*, 128−133.

(2) Kurtz, S. M.; Lau, E.; Watson, H.; Schmier, J. K.; Parvizi, J. Economic Burden of Periprosthetic Joint Infection in the United States. *J. Arthroplasty* **2012**, *27*, 61−65.

(3) Costerton, J. W.; Stewart, P. S.; Greenberg, E. Bacterial Biofilms: A Common Cause of Persistent Infections. *Science* **1999**, *284*, 1318−1322.

(4) Saleh, K. J.; Rand, J. A.; McQueen, D. A. Current Status of Revision Total Knee Arthroplasty: How Do We Assess Results? *J. Bone Joint Surg Am.* **2003**, *85*, S18−20.

(5) Bernard, L.; Hoffmeyer, P.; Assal, M.; Vaudaux, P.; Schrenzel, J.; Lew, D. Trends in the Treatment of Orthopaedic Prosthetic Infections. *J. Antimicrob. Chemother.* **2004**, *53*, 127−129.

(6) Bistolfi, A.; Massazza, G.; Verné, E.; Massè, A.; Deledda, D.; Ferraris, S.; Miola, M.; Galetto, F.; Crova, M. Antibiotic-Loaded Cement in Orthopedic Surgery: A Review. *ISRN Orthopedics* **2011**, *2011*, 290851.

(7) Momentum, R. Single Stage Revision. *J. Bone Joint Surg. Br.* **2012**, *2012*, 120−122.

DOI: 10.1021/acsnano.6b00087
ACS Nano XXXX, XXX, XXX−XXX

(8) Lu, J.; Huang, Z.; Tropiano, P.; d'Orval, B. C.; Remusat, M.; Dejou, J.; Proust, J.-P.; Poitout, D. Human Biological Reactions at the Interface between Bone Tissue and Polymethylmethacrylate Cement. *J. Mater. Sci.: Mater. Med.* **2002**, *13*, 803−809.
(9) Wininger, D. A.; Fass, R. J. Antibiotic-Impregnated Cement and Beads for Orthopedic Infections. *Antimicrob. Agents Chemother.* **1996**, *40*, 2675.
(10) Parvizi, J.; Alijanipour, P.; Barberi, E. F.; Hickok, N. J.; Phillips, K. S.; Shapiro, I. M.; Schwarz, E. M.; Stevens, M. H.; Wang, Y.; Shirtliff, M. E. Novel Developments in the Prevention, Diagnosis, and Treatment of Periprosthetic Joint Infections. *J. Am. Acad. Orthop. Surg.* **2015**, *23*, S32−S43.
(11) Houdek, M. T.; Wagner, E. R.; Watts, C. D.; Osmon, D. R.; Hanssen, A. D.; Lewallen, D. G.; Mabry, T. M. Morbid Obesity: A Significant Risk Factor for Failure of Two-Stage Revision Total Hip Arthroplasty for Infection. *J. Bone Surg.* **2015**, *97*, 326−332.
(12) Pedersen, A. B.; Mehnert, F.; Johnsen, S. P.; Sørensen, H. T. Risk of Revision of a Total Hip Replacement in Patients with Diabetes Mellitus a Population-Based Follow up Study. *J. Bone Jt. Surg., Br. Vol.* **2010**, *92*, 929−934.
(13) Decher, G. Fuzzy Nanoassemblies: Toward Layered Polymeric Multicomposites. *Science* **1997**, *277*, 1232−1237.
(14) DeMuth, P. C.; Min, Y.; Huang, B.; Kramer, J. A.; Miller, A. D.; Barouch, D. H.; Hammond, P. T.; Irvine, D. J. Polymer Multilayer Tattooing for Enhanced DNA Vaccination. *Nat. Mater.* **2013**, *12*, 367−376.
(15) Boudou, T.; Crouzier, T.; Ren, K.; Blin, G.; Picart, C. Multiple Functionalities of Polyelectrolyte Multilayer Films: New Biomedical Applications. *Adv. Mater.* **2010**, *22*, 441.
(16) Lavalle, P.; Voegel, J. C.; Vautier, D.; Senger, B.; Schaaf, P.; Ball, V. Dynamic Aspects of Films Prepared by a Sequential Deposition of Species: Perspectives for Smart and Responsive Materials. *Adv. Mater.* **2011**, *23*, 1191−1221.
(17) Jessel, N.; Atalar, F.; Lavalle, P.; Mutterer, J.; Decher, G.; Schaaf, P.; Voegel, J. C.; Ogier, J. Bioactive Coatings Based on a Polyelectrolyte Multilayer Architecture Functionalized by Embedded Proteins. *Adv. Mater.* **2003**, *15*, 692−695.
(18) Wenke, J. C.; Guelcher, S. A. Dual Delivery of an Antibiotic and a Growth Factor Addresses Both the Microbiological and Biological Challenges of Contaminated Bone Fractures. *Expert Opin. Drug Delivery* **2011**, *8*, 1555−1569.
(19) Goodman, S. B.; Yao, Z.; Keeney, M.; Yang, F. The Future of Biologic Coatings for Orthopaedic Implants. *Biomaterials* **2013**, *34*, 3174−3183.
(20) Gristina, A. G. Biomaterial-Centered Infection: Microbial Adhesion *Versus* Tissue Integration. *Science* **1987**, *237*, 1588−1595.
(21) Hench, L. L.; Polak, J. M. Third-Generation Biomedical Materials. *Science* **2002**, *295*, 1014−1017.
(22) Guelcher, S. A.; Brown, K. V.; Li, B.; Guda, T.; Lee, B.-H.; Wenke, J. C. Dual-Purpose Bone Grafts Improve Healing and Reduce Infection. *J. Orthop. Trauma* **2011**, *25*, 477−482.
(23) Busscher, H. J.; van der Mei, H. C.; Subbiahdoss, G.; Jutte, P. C.; van den Dungen, J. J. A. M.; Zaat, S. A. J.; Schultz, M. J.; Grainger, D. W. Biomaterial-Associated Infection: Locating the Finish Line in the Race for the Surface. *Sci. Transl. Med.* **2012**, *4*, 153rv110.
(24) Nakashima, M.; Reddi, A. H. The Application of Bone Morphogenetic Proteins to Dental Tissue Engineering. *Nat. Biotechnol.* **2003**, *21*, 1025−1032.
(25) Triplett, R. G.; Nevins, M.; Marx, R. E.; Spagnoli, D. B.; Oates, T. W.; Moy, P. K.; Boyne, P. J. Pivotal, Randomized, Parallel Evaluation of Recombinant Human Bone Morphogenetic Protein-2/Absorbable Collagen Sponge and Autogenous Bone Graft for Maxillary Sinus Floor Augmentation. *J. Oral Maxillofac. Surg.* **2009**, *67*, 1947−1960.
(26) Facca, S.; Cortez, C.; Mendoza-Palomares, C.; Messadeq, N.; Dierich, A.; Johnston, A. P. R.; Mainard, D.; Voegel, J. C.; Caruso, F.; Benkirane-Jessel, N. Active Multilayered Capsules for *in Vivo* Bone Formation. *Proc. Natl. Acad. Sci. U. S. A.* **2010**, *107*, 3406−3411.
(27) Petite, H.; Viateau, V.; Bensaid, W.; Meunier, A.; de Pollak, C.; Bourguignon, M.; Oudina, K.; Sedel, L.; Guillemin, G. Tissue-Engineered Bone Regeneration. *Nat. Biotechnol.* **2000**, *18*, 959−963.
(28) Lynn, D. M.; Langer, R. Degradable Poly (B-Amino Esters): Synthesis, Characterization, and Self-Assembly with Plasmid DNA. *J. Am. Chem. Soc.* **2000**, *122*, 10761−10768.
(29) Little, S. R.; Lynn, D. M.; Ge, Q.; Anderson, D. G.; Puram, S. V.; Chen, J.; Eisen, H. N.; Langer, R. Poly-B Amino Ester-Containing Microparticles Enhance the Activity of Nonviral Genetic Vaccines. *Proc. Natl. Acad. Sci. U. S. A.* **2004**, *101*, 9534−9539.
(30) Macdonald, M. L.; Samuel, R. E.; Shah, N. J.; Padera, R. F.; Beben, Y. M.; Hammond, P. T. Tissue Integration of Growth Factor-Eluting Layer-by-Layer Polyelectrolyte Multilayer Coated Implants. *Biomaterials* **2011**, *32*, 1446−1453.
(31) Pashuck, E. T.; Stevens, M. M. Designing Regenerative Biomaterial Therapies for the Clinic. *Sci. Transl. Med.* **2012**, *4*, 160sr164.
(32) Zara, J. N.; Siu, R. K.; Zhang, X.; Shen, J.; Ngo, R.; Lee, M.; Li, W.; Chiang, M.; Chung, J.; Kwak, J. High Doses of Bone Morphogenetic Protein 2 Induce Structurally Abnormal Bone and Inflammation *in Vivo*. *Tissue Eng., Part A* **2011**, *17*, 1389−1399.
(33) Peters, M. C.; Polverini, P. J.; Mooney, D. J. Engineering Vascular Networks in Porous Polymer Matrices. *J. Biomed. Mater. Res.* **2002**, *60*, 668−678.
(34) Shah, N. J.; Hyder, M. N.; Moskowitz, J. S.; Quadir, M. A.; Morton, S. W.; Seeherman, H. J.; Padera, R. F.; Spector, M.; Hammond, P. T. Surface-Mediated Bone Tissue Morphogenesis from Tunable Nanolayered Implant Coatings. *Sci. Transl. Med.* **2013**, *5*, 191ra183.
(35) Uludag, H.; D'Augusta, D.; Palmer, R.; Timony, G.; Wozney, J. Characterization of Rhbmp-2 Pharmacokinetics Implanted with Biomaterial Carriers in the Rat Ectopic Model. *J. Biomed. Mater. Res.* **1999**, *46*, 193−202.
(36) Min, J.; Braatz, R. D.; Hammond, P. T. Tunable Staged Release of Therapeutics from Layer-by-Layer Coatings with Clay Interlayer Barrier. *Biomaterials* **2014**, *35*, 2507−2517.
(37) Li, D.; Gromov, K.; Søballe, K.; Puzas, J. E.; O'Keefe, R. J.; Awad, H.; Drissi, H.; Schwarz, E. M. Quantitative Mouse Model of Implant-Associated Osteomyelitis and the Kinetics of Microbial Growth, Osteolysis, and Humoral Immunity. *J. Orthop. Res.* **2008**, *26*, 96−105.
(38) Cassat, J. E.; Hammer, N. D.; Campbell, J. P.; Benson, M. A.; Perrien, D. S.; Mrak, L. N.; Smeltzer, M. S.; Torres, V. J.; Skaar, E. P. A Secreted Bacterial Protease Tailors the Staphylococcus Aureus Virulence Repertoire to Modulate Bone Remodeling During Osteomyelitis. *Cell Host Microbe* **2013**, *13*, 759−772.
(39) Olson, M. E.; Horswill, A. R. Staphylococcus Aureus Osteomyelitis: Bad to the Bone. *Cell Host Microbe* **2013**, *13*, 629−631.
(40) Lynn, D. M.; Langer, R. Degradable Poly(Beta-Amino Esters): Synthesis, Characterization, and Self-Assembly with Plasmid DNA. *J. Am. Chem. Soc.* **2000**, *122*, 10761−10768.

DOI: 10.1021/acsnano.6b00087
ACS Nano XXXX, XXX, XXX−XXX